Journal of Marine Research, 70, 689–718, 2012

Experimental assessment of particle mixing fingerprints in the deposit-feeding bivalve *Abra alba* (Wood)

by Guillaume Bernard[1,2], Antoine Grémare[1], Olivier Maire[1], Pascal Lecroart[1], Filip J.R. Meysman[3], Aurélie Ciutat[4], Bruno Deflandre[1] and Jean Claude Duchêne[4]

ABSTRACT

Particle mixing induced by the deposit-feeding bivalve *Abra alba* was assessed using a new experimental approach allowing for the tracking of individual particle displacements. This approach combines the adaptation of existing image acquisition techniques with new image analysis software that tracks the position of individual particles. This led to measurements of particle mixing fingerprints, namely the frequency distributions of particle waiting times, and of the characteristics (i.e. direction and length) of their jumps. The validity of this new approach was assessed by comparing the so-measured frequency distributions of jump characteristics with the current qualitative knowledge regarding particle mixing in the genus *Abra*. Frequency distributions were complex due to the coexistence of several types of particle displacements and cannot be fitted with the most commonly used procedures when using the Continuous Time Random Walk (CTRW) model. Our approach allowed for the spatial analysis of particle mixing, which showed: 1) longer waiting times; 2) more frequent vertical jumps; and 3) shorter jump lengths deep in the sediment column than close to the sediment-water interface. This resulted in lower D_b^X and D_b^Y (vertical and horizontal particle mixing bioffusion coefficients) deep in the sediment column. Our results underline the needs for: 1) preliminary checks of the adequacy of selected distributions to the species/communities studied; and 2) an assessment of vertical changes in particle mixing fingerprints when using CTRW.

1. Introduction

Marine benthic macrofauna strongly affect the fate of settled particulate organic matter (POM) through bioturbation (Meysman *et al.*, 2006), which encompasses two distinct processes: 1) bioirrigation (i.e, the enhanced exchange of water and solutes across the sediment-water interface due to burrow ventilation); and 2) particle mixing (i.e., particle movements due the activity of benthic fauna) (Kristensen *et al.*, 2012). Bioirrigation enhances the oxygenation of the sediment and thereby promotes the degradation of POM (Aller and Aller, 1998). Conversely, particle mixing stimulates the transfer of POM to deeper anoxic layers where organic matter degradation processes are less efficient (Kristensen 2000). Particle

1. UNIV. BORDEAUX, EPOC UMR 5805, F33400 Talence, France
2. Corresponding author ***e-mail: g.bernard@epoc.u-bordeaux1.fr***
3. The Royal Netherlands Institute of Sea Research (NIOZ) Korringaweg 7, 4401 NT Yerseke, The Netherlands
4. CNRS EPOC UMR 5805, F33400 Talence, France

mixing results from burrowing, feeding, defecation and locomotion (Meysman *et al.*, 2006). It occurs globally across the ocean floor, and is of particular importance in areas where physical disturbance is low (Lecroart *et al.*, 2010). Benthic communities change along disturbance gradients (Pearson and Rosenberg, 1978) together with rates of particle mixing. These changes generate a complex interplay between benthic fauna and both the quantity and quality of organic matter, which strongly affects the physical, chemical and geotechnical properties of marine sediments (Rhoads, 1974; Aller, 1982; Rhoads and Boyer, 1982; Meadows and Meadows, 1991; Gilbert *et al.*, 1995; Rowden *et al.*, 1998; Lohrer *et al.*, 2004). Unravelling these interactions requires an improvement of the methods currently used for quantifying particle mixing (Maire *et al.*, 2008).

Particle tracer methods are the most widely used and all rely on the same steps: 1) the deposition of tracer particles at the sediment-water interface; 2) the determination of tracer vertical profiles within the sediment column; and 3) the computation of particle mixing rates by fitting mixing models to those profiles. The most widely implemented model is the biodiffusion model, which assumes that Fick's first law of diffusion is applicable to tracer dispersion (Guinasso and Schink, 1975; Boudreau, 1986a; Wheatcroft *et al.*, 1992; Gérino *et al.*, 1998). It is easy to implement and results in a single parameter that quantifies the rate of particle mixing: the biodiffusion coefficient (D_b). The biodiffusion model has often proved suitable to fit tracer profiles (Lecroart *et al.*, 2007, 2010), which constitutes a paradox since its main assumptions (*i.e.*, non-oriented, extremely frequent and extremely small particle displacements) are most often not fulfilled (Meysman *et al.*, 2003).

More sophisticated models have been developed that claim to have a stronger biological background (e.g. Boudreau, 1986b; Robbins, 1986; Boudreau and Imboden, 1987; Soetaert *et al.*, 1996; François *et al.*, 2002). These so-called non-local models are more difficult to handle from a mathematical standpoint. It is also more difficult to acquire appropriate data to evaluate them. This explains why they have only been implemented occasionally (Rice, 1986; Shull, 2001; Solan *et al.*, 2004; Delmotte *et al.*, 2007). Meysman *et al.* (2008a, 2008b and 2010) proposed the CTRW model to describe particle mixing. In this model, the effect of mixing is assessed by tracking the elementary motion of individual particles. Particle displacement is described as a random process, and is governed by three stochastic variables: 1) the jump direction; 2) the jump length; and 3) the waiting time between two consecutive jumps of the same particle (Wheatcroft *et al.*, 1990). Overall, the joined frequency distributions of these variables form the "mixing fingerprint" of a benthic community or a benthic organism (Meysman *et al.*, 2008a). Meysman *et al.* (2008b) have developed a one-dimensional CTRW model, in which particle displacement is governed by two frequency distribution functions describing the waiting times (typically a Poisson process) and the vertical components of jump lengths (typically a Gaussian distribution). This approach was shown to have advantages over the simple biodiffusion model in describing tracer profiles generated by the bivalve *Abra ovata* (Maire *et al.*, 2007a). It has also been used successfully with the bivalve *A. alba*, the polychaete *Nephtys sp.* (Braeckman *et al.*, 2010) and the amphipod *Corophium volutator* (De Backer *et al.*, 2011). The application of the CTRW

model however remains limited due to its mathematical complexity. Moreover, even if it constitutes a progress relative to the biodiffusive model, the *a priori* selection of simple functions to describe the frequency distributions of waiting times and jump lengths remains unverified (Meysman *et al.*, 2010).

Tracer profiles are classically determined by slicing sediment cores and subsequently quantifying the tracer within each sediment layer. Artificial tracers such as glass beads and luminophores are quantified using image acquisition and analysis techniques (Maire *et al.*, 2008). The combination of these approaches have been successfully used to quantify particle mixing both by benthic communities (Gilbert *et al.*, 2003; Solan *et al.*, 2004) and individual species (Maire *et al.*, 2006, 2007a, 2007b; Piot *et al.*, 2008). The use of transparent aquaria allows for a two-dimensional dynamic view of particle mixing (Maire *et al.*, 2006, 2007a, 2007b). Recent technological advancements (increase the frequency of image capture) allow for a direct assessment of waiting time frequency distributions. Similar possibilities exist for jump lengths and directions. Maire *et al.* (2007c) have developed a specific algorithm to assess the displacements of sediment particles along the tentacles of the deposit-feeding polychaete *Eupolymnia nebulosa* that can indeed be transposed to the analysis of luminophore trajectories.

A major challenge in particle mixing research is to get accurate estimates of mixing fingerprints (Reed *et al.*, 2006; Maire *et al.*, 2007a; Meysman *et al.*, 2008a, 2008b). This has not been achieved yet due to technical limitations. The aim of the present study is to adapt existing image analysis techniques to experimentally assess the frequency distributions of: 1) waiting times; 2) jump directions; and 3) jump lengths to describe sediment particle mixing by the bivalve *A. alba*.

2. Materials and methods

a. Bivalve collection and maintenance

The deposit-feeding bivalve *Abra alba* belongs to the super family Tellinoidea. It is a dominant macrobenthic species in shallow subtidal areas along the European Atlantic coast (Borja *et al.*, 2004; Van Hoey *et al.*, 2005). It is abundant and a dominant species in the Arcachon Lagoon where abundances can reach up to 500 individuals.m^{-2} and shell lengths are typically between 5 and 15 mm (Blanchet *et al.*, 2005). Its body is usually buried a few centimeters below the sediment surface (Braeckman *et al.*, 2010). It reworks the upper layer of the sediment when feeding. Foraging movements typically consist of circular motions of the tip of the inhalant siphon at the sediment-water interface (Hughes, 1975).

During the present study, sediment samples were collected in June 2010 and May 2011 in the Courbey Channel (45° 43′476 N, 1° 37′758 W, 3–5 m depth, Arcachon Bay, France) using a Van-Veen grab. Samples were passed through a 1 mm mesh, yielding ∼500 clams (9-12 mm shell length). Additional grabs were passed through a 1 mm sieve to remove macrofauna. This sediment (47.7 % sand and 52.3 % fines; 1.40 % POC and 0.16 % PON) was used both for maintenance and experimentation. Clams were kept in tanks (60 × 40 × 30 cm) filled

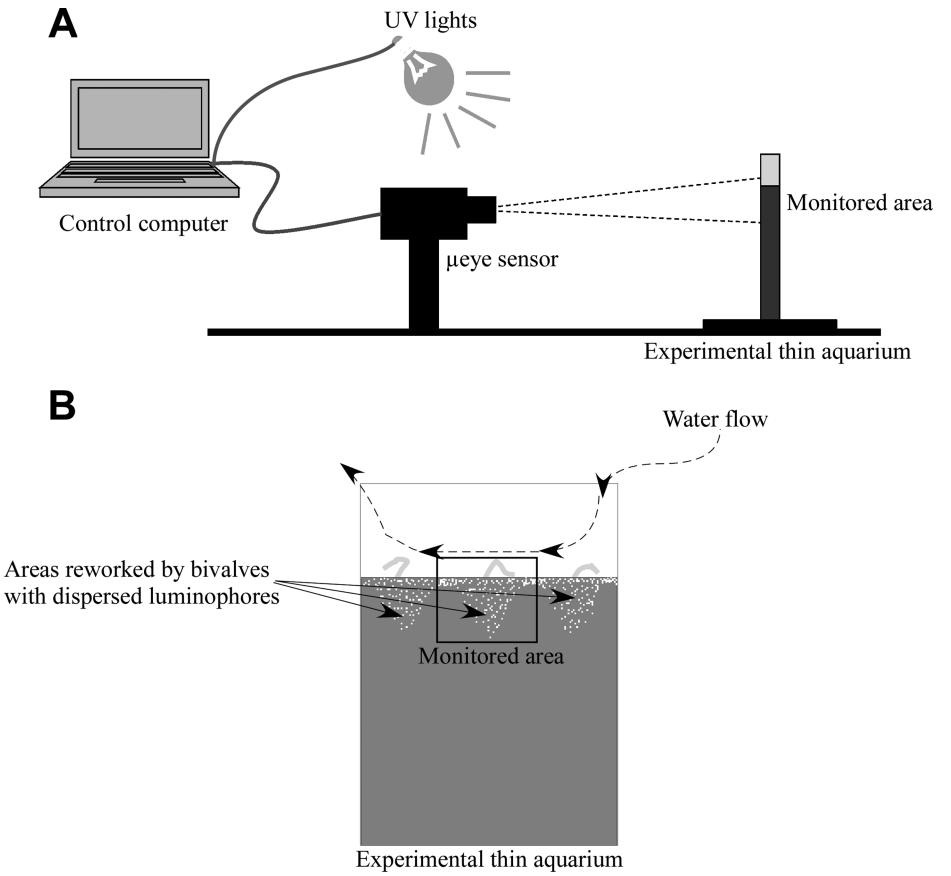

Figure 1. Lateral (A) and frontal (B) views of the setup used during the eight experiments.

with field sediment and supplied with ambient running seawater prior to experimentation. They were fed once a week with crushed Tetramin® fish food (4.59 gPOC.week^{-1}).

b. Experimental set-up

The experimental set-up (Fig. 1) was modified from Maire *et al.* (2006). Thin aquaria (L = 17 cm, W = 0.9 cm, H = 33 cm) were filled with 15 cm of field sediment and kept at ambient seawater temperature for three days before each experiment. Three clams of known size were then gently placed at the sediment surface, after which they typically buried within 30 seconds. After 24 hours, 1.5 g of yellow luminophores (Ecotrace, Environmental Tracing®, median diameter = 35 μm) were spread at the sediment surface. Aquaria were placed in front of two UV lights (λ = 365 nm, which allowed for the distinction between fluorescent luminophores and the surrounding sediment) and of a μ eye video

captor (IDS®, definition of $2,560 \times 1,920$ pixels). The monitored field was 4.2 cm $\times$ 3.2 cm, which resulted in a resolution of 16.5 μm.pixel^{-1}. The experiment began 24 hours after luminophore introduction. This allowed for: 1) the monitored field to be centred on an area reworked by a single bivalve; and 2) the dispersion of luminophores. Each experiment lasted 48 hours and image frequency acquisition was 0.1 Hz. The series of images collected during each experiment were assembled in an AVI video format. We will report on the results of eight replicated experiments. Seven were carried out between June 22 and Sept. 24, 2010 with temperatures between 19.2 and 21.3°C and one on June 16, 2011 at a temperature of 21.2°C.

c. Image processing

AVI films were processed using two specific algorithms that track the position of individual luminophores within consecutive images. The goal was to categorize the motion of individual particles following the CTRW formalism. Only the movements of isolated luminophores make sense in such an analysis. Isolated luminophores were first binarised in each individual image based on their red-green-blue levels, luminance and size. The (XY) coordinates of their barycentre was taken as representative for their position. Waiting times and jump characteristics algorithms were both implemented in a specific software (Obvious AviExplore), which was developed using Microsoft Visual Studio C#.

The algorithm that describes a waiting event is presented in Figure 2a. A given particle "waits" if it does not move outside of a sensitivity circle. This sensitivity circle accounts both for changes in the apparent size of the luminophores due to fluctuations in light intensity, and for small movements due to vibrations. Here, we used a radius of 66 μm for the sensitivity circle (four pixels). This value was based on the apparent size of luminophores including halos (typically $\sim$50 μm radius or three pixels), and the displacements of "fixed" reference spots that were painted on the wall of the aquaria. The waiting event algorithm works as follows: imagine that at time t, a luminophore has been waiting for m time intervals. If at time $t + 1$, the position of the luminophore is still located within the sensitivity circle, we assume there has been no jump between time t and $t + 1$, and the waiting event continues. The (XY) coordinates are updated, and the waiting time is incremented (i.e., set to $m + 1$). Conversely, if the position of the luminophore at time $t + 1$ is located outside the sensitivity circle, the luminophore has jumped between time t and $t + 1$. The waiting time event has ended and its waiting time is determined as being m time intervals. When a waiting time event has ended, the following parameters are recorded: the index number of the starting image (corresponding to the arrival of the luminophore at its initial position), the index number of the final image (corresponding to the jump of the luminophore to its new position), the waiting time, and the (XY) coordinates of the luminophore in the final image.

The algorithm that analyses the jumps is presented in Figure 2b. It accounts for the fact that a particle jump does not necessarily occur within the monitored plane, which complicates

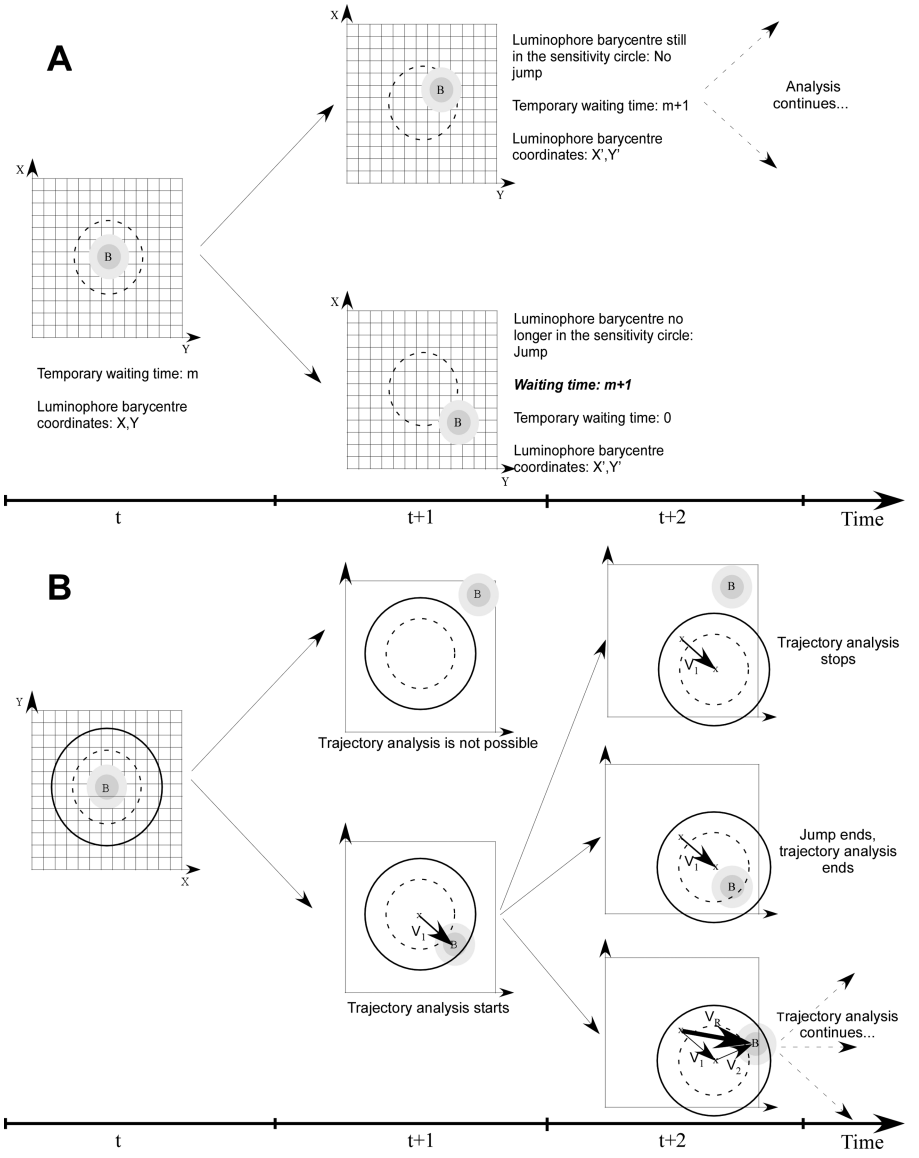

Figure 2. Principles used for the computation of waiting times (A). The two centered gray circles are the luminophore and its halo positions. B is the barycentre of the luminophore. The open circle with a dotted line is the sensitivity circle (see text for details). Principles used for the computation of jump lengths and directions (B). The two centered gray circles are the luminophore and its halo positions. B is the barycentre of the luminophore. The open circle with a continuous line is the search circle. The open circle with a dotted line is the sensitivity circle (see text for details).

the tracking of particles. A given particle "jump" can be characterized if the considered particle moves outside of a sensitivity circle, but stays within a broader search circle. The delineation of a search circle is needed to ensure the same particle is tracked in consecutive images. Here, we used a value of 660 μm for the radius of the search circle. This value was determined in calibration tests on selected video sections, where we optimized the automatic detection of luminophore movements by visually following particle movements. The jump event algorithm works as follows: imagine that a particle jumped between t and $t + 1$ (i.e. the particle is present with the sensitivity circle at time t, but no longer present within the sensitivity circle at time $t + 1$). There are multiple possibilities at time $t + 1$. If there is no particle present between the sensitivity and search circles, then it is assumed that the particle disappeared from the wall and moved into the interior of the aquarium and no trajectory analysis can be performed. If one particle is present between the sensitivity and search circles, this is regarded as the new position of the particle (note when several particles are present within the search circle, we select the particle with the position closest to the original location). We then can draw a vector V_1 that links the positions at time t and time $t + 1$. The trajectory analysis starts. If the same luminophore moves during more than two consecutive images, this is considered a single jump. V_1 forms the first element of the corresponding trajectory. The analysis then continues at time $t + 2$ with three alternative possibilities:

1) There is a particle within the sensitivity circle centered on the luminophore's position at time $t + 1$. This is most likely the original particle which has not moved. The jump ended, and the duration of the jump is a one time interval. The overall jump vector is the vector V_1.
2) There is no particle within the search circle centered on the luminophore's position at time $t + 1$. It is assumed that the particle has disappeared from the wall and moved into the aquarium. The trajectory analysis is stopped. The duration of the jump is a one time interval and the overall jump vector is vector V_1.
3) There is one particle located between the sensitivity and search circles centered on the luminophore's position at time $t + 1$ (here again, when several particles are present within the search circle, we select the particle with the position closest to the location at time $t + 1$). The jump is continuing. The displacement is described by the vector V_2, which links the positions of the particle at times $t + 1$ and $t + 2$. The duration of the jump is set to two time intervals. The overall jump vector between times t and $t + 2$ is computed as the sum of vectors V_1 and V_2. The trajectory analysis then continues at time $t + 3$ with the three above mentioned possibilities.

When a jump event ends, the following parameters are recorded: the index numbers of the starting and final images, the duration of the jump, the (XY) coordinates at the start of the jump, the (XY) coordinates at the end of the jump, the length and the direction of the jump vector.

Jumps can last for more than a single time interval and jump lengths can therefore be longer than the search radius. This approach, however potentially undersamples large jumps, but has the benefits that it: 1) avoids false positives (i.e., characterization of jumps that have not truly occurred); and 2) provides an objective way to track particle displacements. It should also be underlined that the total number of jumps, the numbers of waiting times, and analysed jumps are not necessarily equal. A jump is indeed recorded whenever a luminophore disappears from its sensitivity circle, whereas it can be analysed only if it remains within its search circle between two consecutive images. Furthermore, the determination of a waiting time requires that both the arrival and the departure times of a luminophore at a given position are known.

d. Data processing

i. *Frequency distributions.* Overall, we were able to measure 3,062,006 waiting times and to characterize 1,462,337 jumps. For each experiment, these data (e.g. 570,249 waiting times and 284,361 characterized jumps for Exp. 3) were used to compute the overall frequency distributions of: 1) waiting times; 2) jump lengths; 3) jump directions; 4) the lengths of the vertical and horizontal components of jump vectors; and; 5) jump durations.

ii. *Overall mean values.* The number of jumps detected in a given area is depending not only on particle mixing intensity, but also on the number of luminophores present. The normalized (i.e., divided by the number of luminophores counted in the area) number of jumps represents the probability of jump of a luminophore within the considered area. Our results showed that: 1) all the components of particle mixing fingerprints vary with depth within the sediment column; and 2) the vertical profiles of the total and normalized numbers of jumps strongly differ. The assessment of the overall values of a component of particle mixing fingerprints directly derived from the sets of measured jumps and waiting times would thus be biased due to a "luminophore density effect." The computations of overall mean values of the waiting time, jump length characteristics, and particle tracking biodiffusion coefficients were therefore based on a bootstrap procedure involving 1,000 re-samplings stratified relative to depth. The vertical frequency distributions of the number of resampled events were kept strictly identical to those of the normalized numbers of jumps. The number of jumps per re-sampling was set to limit oversampling and therefore varied according to parameters and experiments.

iii. *Two-dimensional Spatial analysis.* The monitored sediment area was divided into cells of 660 × 660 μm (i.e. 40 × 40 pixels), thus resulting in a two-dimensional grid of 64 × 48 cells. For each cell, we computed: 1) the total number of jumps; 2) the normalised number of jumps; 3) the mean waiting time (T_c); 4) the mean length of the vertical and horizontal components of the jump vectors; 5) the variances (σ_X^2 and σ_Y^2) of the vertical and horizontal components of jump vectors; and 6) the

vertical/horizontal particle-tracking biodiffusion coefficients (D_b^X and D_b^Y). D_b^X was computed in each cell after Meysman *et al.* (2008a):

$$D_b^X = \sigma_x^2/(2T_c).$$

A similar formula applied to the computation of D_b^Y.

iv. *Vertical profiles.* The sediment-water interface was determined based on the location (i.e., maximum X coordinates within each cell column) of the cells where waiting times were recorded. It was then flattened by vertically translating cell columns so the sediment-water interface corresponds to the first row of each column (Solan *et al.*, 2004 ; Maire *et al.*, 2006). The cell X-position in the picture then corresponded directly to its depth within the sediment column. We computed one-dimensional vertical profiles by considering the subsets of individual jumps and/or waiting times occurring within each 660 μm depth interval. This resulted in vertical profiles of: 1) total numbers of jumps; 2) normalized numbers of jumps; 3) mean waiting times; 4) proportions of perfectly vertical jumps (i.e., jumps with an origin and an endpoint within the same pixel column); 5) means lengths of the vertical and horizontal components of jump vectors; 6) σ_X^2 and σ_Y^2; and 7) D_b^X and D_b^Y. The effects of depth on all these parameters were assessed using non-parametric Kruskal-Wallis ANOVAs. Differences between vertical frequency distributions of the total number of jumps and of the normalized number of jumps were assessed using a Kolgomorov-Smirnov test. For each experiment, and based on their vertical profiles, the relationship between D_b^Y and D_b^X was assessed using a simple linear correlation model.

All computations were carried out using specific routines in the open source *R* programming framework v2.13.1. (www.R-project.org, 2011). Statistical analyses were carried out using the SigmaStat® 11.0 software.

3. Results

a. Classification of luminophore movements

Through visual inspection of the 384 hours of video footage, we were able to distinguish between two types of luminophore movements. The first one corresponded to an upward displacement, immediately followed by a downward one. These vertical oscillations were caused by the protrusion/retraction of the foot outside/inside the shell (Figs. 3a, b). They were also detected during inhalant siphon foraging and ejection of faeces or pseudofaeces via the exhalant or the inhalant siphon, respectively (Figs. 3c, d). Since upward displacements were immediately followed by downward ones, this typically resulted in overall jump vectors with a length close to zero. The second type of particle movement was preferentially oriented along the axis of siphonal galleries. Upward movements were caused by the extension of the siphons, which induced luminophore jumps through friction (Fig. 3e). Similarly, downward jumps were caused by siphon retraction (Fig. 3f). Corresponding jump lengths

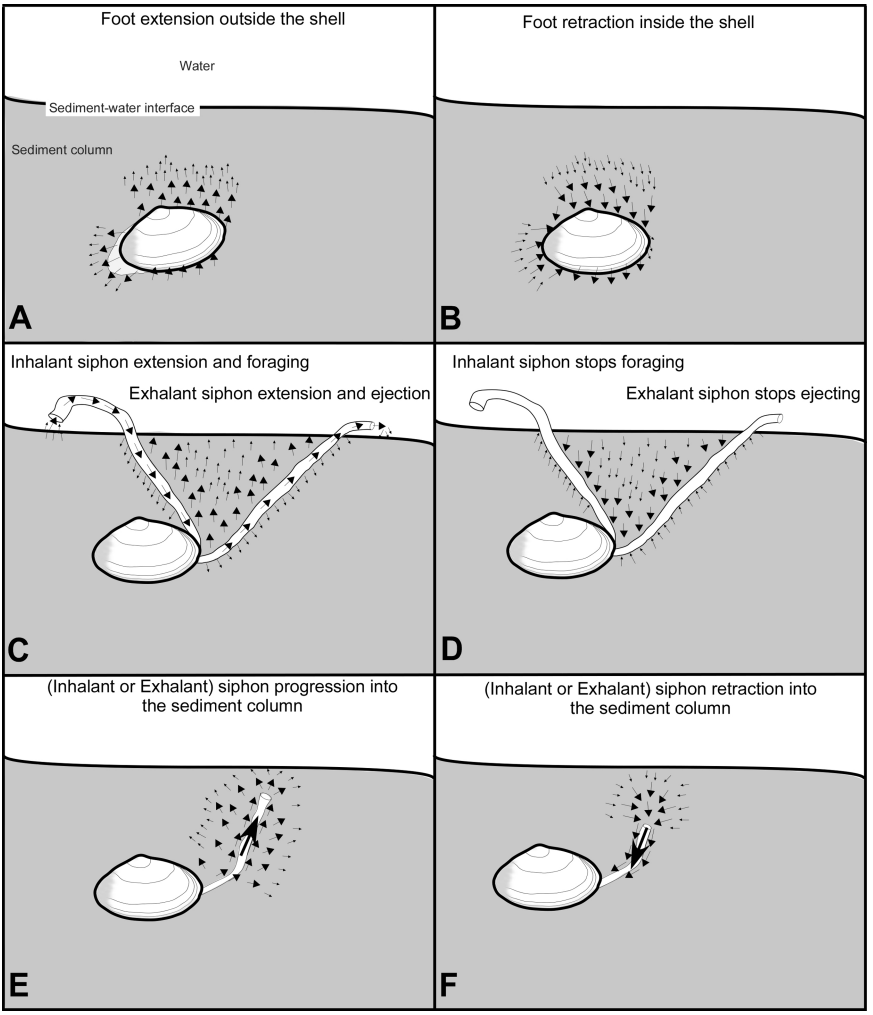

Figure 3. Description of the luminophore displacements induced by different types of behaviours.

usually differed from zero and their vertical components could be either negative (upward jumps) or positive (downward jumps).

b. Frequency distributions

The frequency distribution of waiting times during Experiment 3 was dominated by short values (i.e., 31.8% $\leq$ 1 minute, Fig. 4a). The right tail of this distribution was long and the maximal waiting time was 47.8 hours. For each experiment, these distributions were fitted assuming a Poisson process (Table 1). r^2 were between 0.119 (Exp. 7, $p < 0.0001$) and 0.722 (Exp. 4, $p < 0.0001$) and τ_c between 0.32 hours (Exp. 7) and 1.16 hours (Exp. 2).

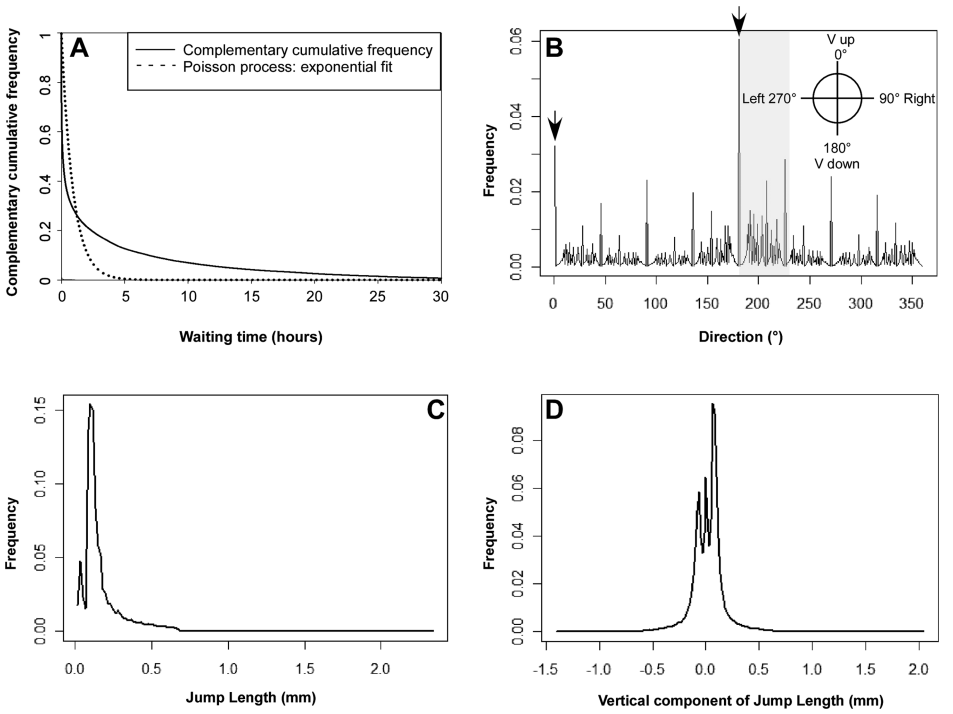

Figure 4. Experiment 3. Frequency distributions of waiting times (A), jump directions (B), jump lengths (C), and vertical components of lengths (D) (positive values are downward, negative values are upward). The shaded area in B indicates a preferential jump orientation (see text for details). Arrows indicate perfectly vertical downward (180°) and upward (0°) jumps. V up: vertical upward, V down: vertical downward.

Table 1. Fits of waiting times distributions assuming a Poisson process. r^2: determination coefficient, p: significance level, τ_c: fitted mean waiting (i.e., assuming a Poisson process for waiting times).

Experiment	Exp. 1	Exp. 2	Exp. 3	Exp. 4	Exp. 5	Exp. 6	Exp. 7	Exp. 8
$\mathbf{r^2}$	0.509	0.674	0.292	0.722	0.376	0.341	0.119	0.175
p	<0.0001	<0.0001	<0.0001	<0.0001	<0.0001	<0.0001	<0.0001	<0.0001
$\boldsymbol{\tau_c}$**(h)**	0.73	1.16	0.92	0.65	1.11	0.93	0.32	1.39

The frequency distribution of jump directions during Experiment 3 (Fig. 4b) was polymodal. Downward jumps were more frequent (56.5%) than upward ones (38.7%). Horizontal jumps accounted for only 4.8%. Together with the vertical (both downward and upward), another preferential jump direction was comprised between 180 and 225°, which corresponded to the preferential orientation of the inhalant siphon within its gallery network during the monitored period. The relative maxima observed at 45, 90, 135, 225, 270 and

315° corresponded to the fact that they were, together with 0 and 180°, the only possible directions for luminophore jumps of short (i.e., < 2 pixels) length.

The frequency distribution of jump lengths during Experiment 3 was bimodal (Fig. 4c), with modes corresponding to a jump length of 0.016 and 0.082 mm, respectively. The frequency distribution of the vertical component of jump lengths during Experiment 3 was trimodal (Fig. 4d), with a first mode (0.066 mm) corresponding to downward jumps, a second one (0 mm) corresponding to a null vertical component of jump lengths (which can either correspond to perfectly horizontal jumps or to jumps lasting for several time intervals with an overall resulting vertical component of jump length of zero), and a third one (−0.066 mm) corresponding to upward jumps.

The frequency distributions during the seven other experiments were similar, although the relative magnitudes of modes slightly differed between experiments.

c. Overall mean values

Overall mean waiting times were between 0.86 hours (Exp. 4) and 2.15 hours (Exp. 3) (Table 2), which led to an overall mean of 1.75 hours with a standard deviation of 0.41 hours and a variation coefficient of 23.5%.

σ_X^2 were between 0.009 (Exp. 4) and 0.033 mm^2 (Exp. 3) (Table 2), which led to an overall mean of 0.024 mm^2 with a standard deviation of 0.007 mm^2 and a coefficient of variation of 29.9%. σ_Y^2 were between 0.011 (Exp. 4) and 0.027 mm^2 (Exp. 6), which led to an overall mean of 0.019 mm^2 with a standard deviation of 0.005 mm^2 and a coefficient of variation of 26.8%).

D_b^X were between 0.486 (Exp. 1) and 0.707 $cm^2.year^{-1}$ (Exp. 8) (Table 2), which led to an overall mean of 0.587 $cm^2.year^{-1}$ with a standard deviation of 0.09 $cm^2.year^{-1}$and a variation coefficient of 15.0%. D_b^Y were between 0.355 (Exp. 1) and 0.559 $cm^2.year^{-1}$ (Exp. 4), which led to an overall mean of 0.491 $cm^2.year^{-1}$ with a standard deviation of 0.081 $cm^2.year^{-1}$ and a variation coefficient of 16.5%.

d. Two-dimensional spatial analysis

The spatial distributions of luminophores at the beginning and end of Experiment 3 are shown in Figures 5a and b, respectively. The initial image was taken 24 hours after a layer of luminophores was deposited at the sediment-water interface, and still showed large patches of luminophores that have not been displaced. Most of these patches were dispersed during the next 48 hours, and the luminophores tended to be homogenously distributed at the end of the experiment (Fig. 5b). However, the subsurface patches on the right side of image remained almost unaffected, indicating an area that was not reworked by the siphon activity of the clams. Also note that the sediment-water interface was not initially flat due to bivalve activity during the 24 hours preceding the experiment and then had a tendency to flatten out during the course of the experiment.

The spatial distribution of the number of jumps during Experiment 3 showed that jumps: 1) occurred over the whole Y axis of the monitored area; and 2) were scarcer at depth,

Table 2. Overall mean values of waiting times, jump characteristics, D_b^Y and D_b^X during our 8 experiments (see text for details on the computation procedure). Data from Braeckmann *et al.* (2010) are provided for comparison. Tc: waiting time, $\sigma^2_{X/Y}$: variance of vertical/horizontal components of jump lengths, $D_b^{X/Y}$: vertical/horizontal particle-tracking biodiffusion coefficient. NF: No Food added.

Species	T_c(h)	σ^2_Y (mm^2)	D_b^Y($cm^2.yr^{-1}$)	σ^2_X (mm^2)	D_b^X($cm^2.y^{-1}$)	Reference
Abra alba (20.4° C, NF, Ex 1)	2.12	0.017	0.355	0.024	0.486	Present study
Abra alba (20.6° C, NF, Ex 2)	1.78	0.018	0.447	0.024	0.588	Present study
Abra alba (21.3° C, NF, Ex 3)	2.15	0.026	0.538	0.032	0.668	Present study
Abra alba (20.7° C, NF, Ex 4)	0.86	0.011	0.559	0.009	0.490	Present study
Abra alba (20.4° C, NF, Ex 5)	1.84	0.018	0.437	0.024	0.570	Present study
Abra alba (19.2° C, NF, Ex 6)	1.99	0.027	0.591	0.030	0.673	Present study
Abra alba (19.8° C, NF, Ex 7)	1.68	0.017	0.446	0.020	0.511	Present study
Abra alba (21.2° C, NF, Ex 8)	1.58	0.020	0.552	0.025	0.707	Present study
Abra alba (10° C, NF, density: 382.m^{-2})	–	–	–	–	1.73-1.82	Braeckmann *et al.* (2010)
Abra alba (10° C, NF, density: 764.m^{-2})	–	–	–	–	2.36-3.63	Braeckmann *et al.* (2010)
Abra alba (10° C, NF, density: 1273.m^{-2})	–	–	–	–	4.47	Braeckmann *et al.* (2010)
Abra alba (18° C, NF, density: 382.m^{-2})	–	–	–	–	0.96	Braeckmann *et al.* (2010)
Abra alba (18° C, NF, density: 764.m^{-2})	–	–	–	–	1.98-3.40	Braeckmann *et al.* (2010)
Abra alba (18° C, NF, density: 1273.m^{-2})	–	–	–	–	3.44-4.22	Braeckmann *et al.* (2010)

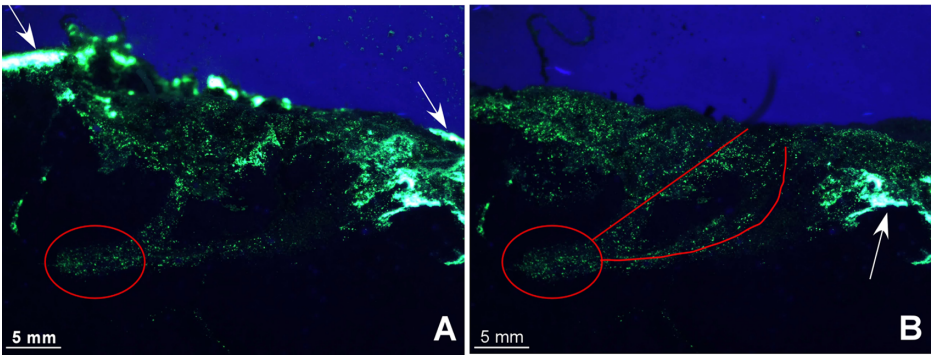

Figure 5. Experiment 3. Photographs showing the two-dimensional spatial distributions of luminophores at the beginning (A) and the end of the experiment (B). Arrows indicate remains of the layer of luminophores initially deposited at the sediment-water interface (A) and an unaffected blob of luminophores (B). Circles indicate the location of the shell and red lines show the location of the two preferentially used galleries (B). See text for details.

where they predominantly occurred in the area close to the bivalve (Fig. 6a). The spatial distributions differed between the total and the normalized number of jumps, although there was also a clear tendency toward a decrease in the normalized number of jumps with increasing depth within the sediment column (Fig. 6b and Fig. 9a).

The spatial distribution of waiting times during Experiment 3 is shown in Figure 6c. The shortest waiting times were found at the sediment-water interface and in siphonal galleries, while longer ones were found just below this interface in two distinct zones located outside the galleries network on the left and on the right (Fig. 6c).

The spatial distributions of: 1) the absolute values of vertical components of jump vectors; 2) the absolute values of horizontal components of jump vectors; 3) σ_X^2; and 4) σ_Y^2 are shown in Figures 7a, 7b, 7c and 7d, respectively. Absolute values of the vertical components of jump vectors were maximal close to the sediment-water interface and then progressively decreased with depth to reach a minimal value close to the location of the shell (Fig. 7a). Absolute values of vertical components of jump vectors, together with σ_X^2 and σ_Y^2 followed the same pattern (Figs. 7b, c and d, respectively). This general gradient was altered by the presence of two preferential siphonal galleries characterized by larger vertical and/or horizontal components of jump vectors and higher σ_X^2 and σ_Y^2 than surrounding sediment. D_b^X and D_b^Y (Figs 8a, b) were high close to the sediment-water interface and within the preferential siphonal galleries. Conversely, they were low in the area surrounding the shell and outside the network of siphonal galleries.

e. Vertical profiles

The vertical frequency distributions of the total number of jumps and of the normalized number of jumps are shown in Figure 9a. These two distributions differed significantly

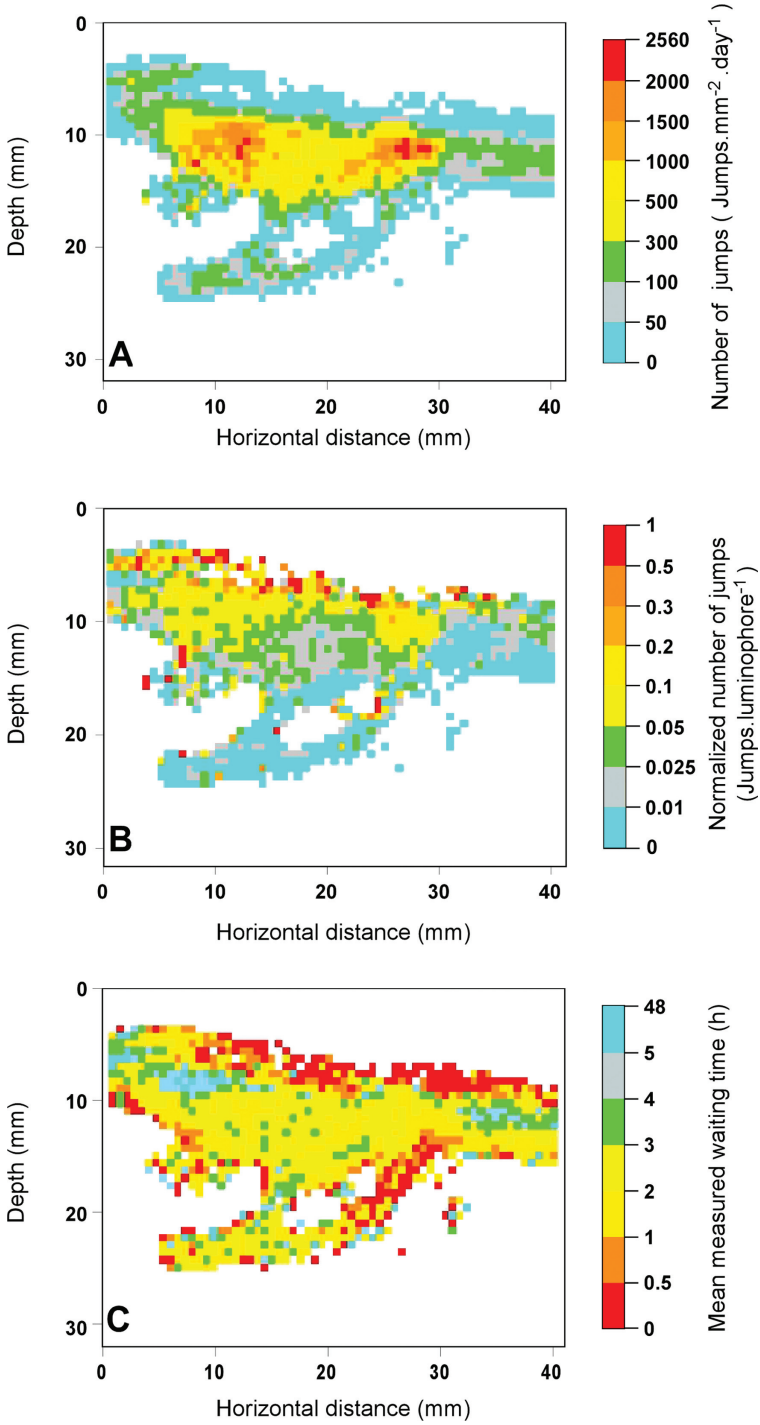

Figure 6. Experiment 3. Two-dimensional maps of the numbers of jumps (A), the normalized numbers of jumps (B), and waiting times (C). White areas correspond to cells where no event was detected.

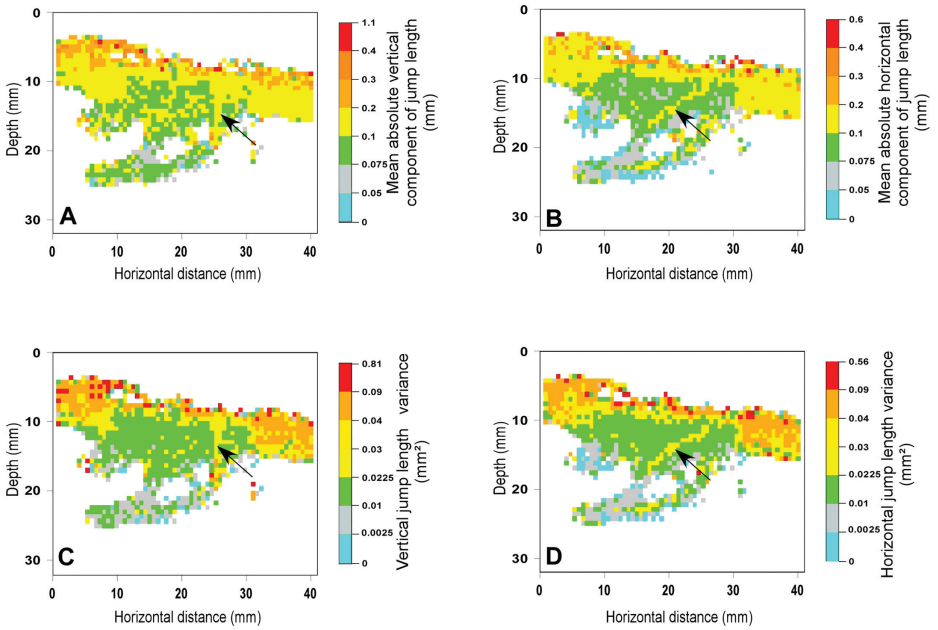

Figure 7. Experiment 3. Two-dimensional maps of: means of absolute vertical (A) and horizontal (B) components of jump lengths; σ^2_X (C) and σ^2_Y (D). Arrows indicate the localisation of the most active siphonal galleries. White areas correspond to cells where no event was detected.

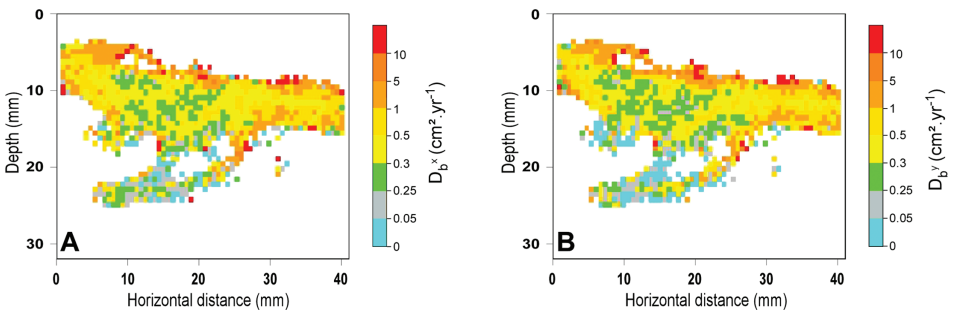

Figure 8. Experiment 3. Two-dimensional maps of D_b^X (A) and D_b^Y (B). White areas correspond to cells where no D_b could be computed due to the lack of detected events.

(Kolgomorov-Smirnov test, $p < 0.001$). Total number of jumps showed a sharp maximum 5 mm deep in the sediment column, whereas normalized number of jumps tended to be higher within the first 5 mm below the sediment-water interface. Both parameters then decreased to reach almost null values 12 mm deep in the sediment.

During Experiment 3, all the parameters listed below were significantly affected by depth within the sediment column (non-parametric Kruskal-Wallis ANOVAs, $p < 0.001$ in all

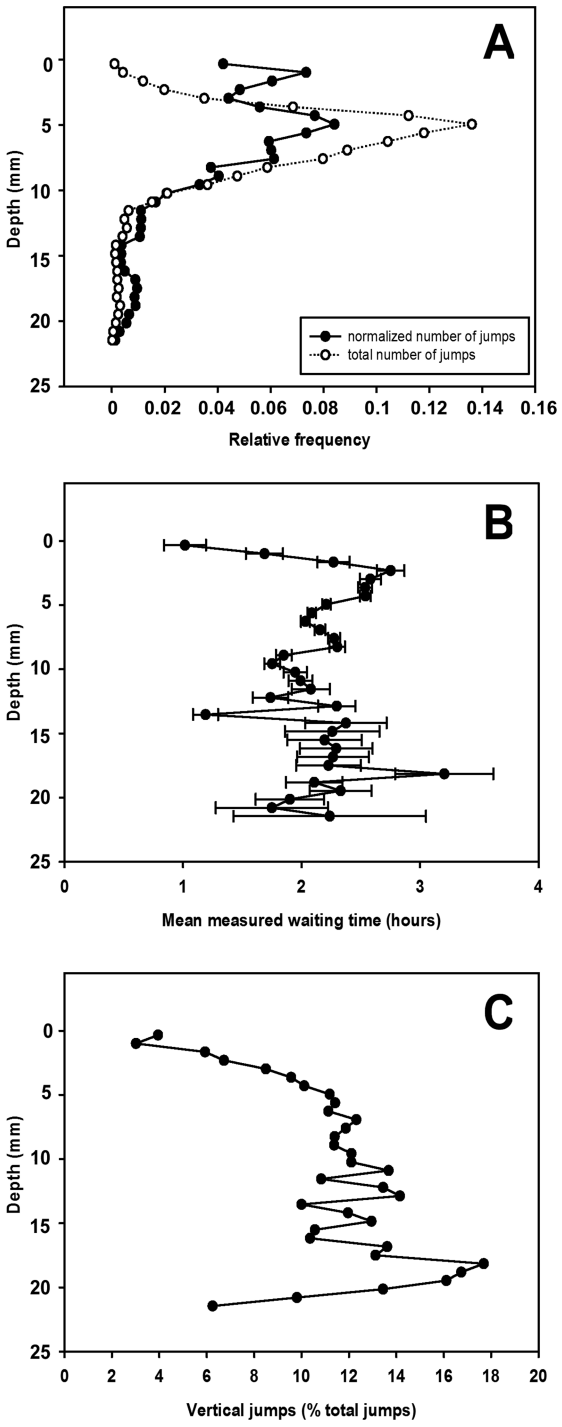

Figure 9. Experiment 3. Vertical profiles of: the relative frequencies numbers and normalized numbers of jumps (A), waiting times (B), and proportions of perfectly vertical jumps (C). Horizontal bars are 95% confidence intervals.

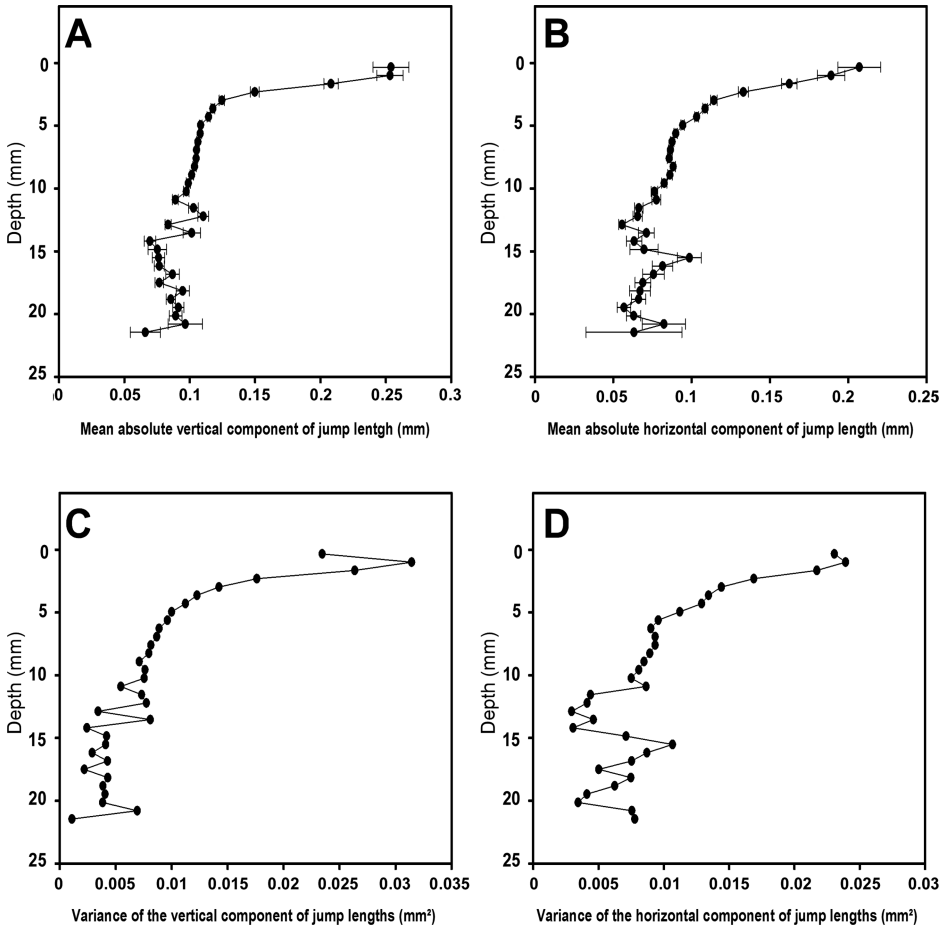

Figure 10. Experiment 3. Vertical profiles of: means of absolute vertical (A) and horizontal (B) components of jump lengths, σ^2_X (C) and σ^2_Y (D). Horizontal bars are 95% confidence intervals.

cases). Waiting times first tended to increase with depth within the sediment column to reach a maximum of ca. 3 hours at a 2 mm depth (Fig. 9b). They then progressively decreased to ca. 2 hours 10 mm deep in the sediment. Values below 10 mm were characterized by large confidence intervals resulting from the low number of jumps deep in the sediment.

The proportion of perfectly vertical jumps tended to increase with depth within the sediment column (Fig. 9c). It was about 3% close to the sediment interface versus 12-14 % deep in the sediment. Absolute values of both the vertical and the horizontal components of jump vectors tended to decrease with depth (Figs. 10a,b). Vertical components decreased from 0.260 close to the sediment-water interface to ca. 0.080 mm deep in the sediment (Fig. 10a), versus ca. 0.220 to 0.060 mm for horizontal ones (Fig. 10b). Corresponding

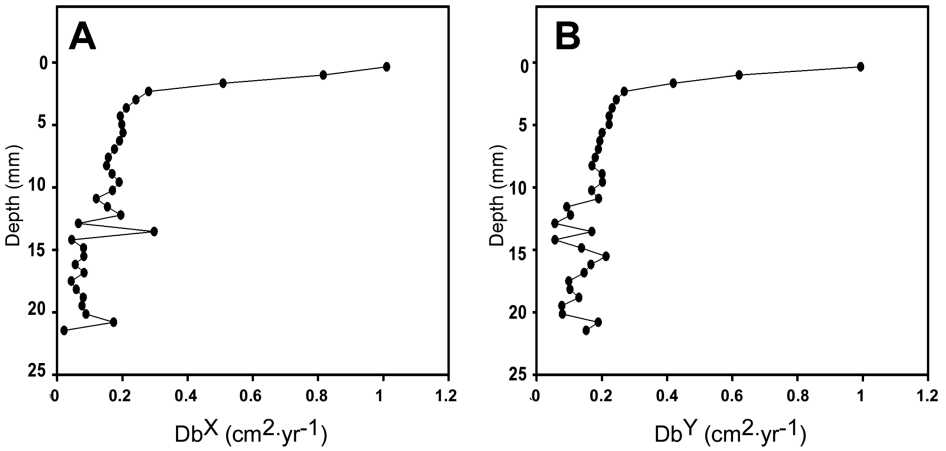

Figure 11. Experiment 3. Vertical profiles of D_b^X (A) and D_b^Y(B).

Table 3. Relationships between D_b^Y and D_b^X as assessed by using simple linear correlation models. r^2: determination coefficient, a: slope, y_0: Y-intercept, p: significance level.

Experiment	Exp. 1	Exp. 2	Exp. 3	Exp. 4	Exp. 5	Exp. 6	Exp. 7	Exp. 8
r^2	0.82	0.64	0.91	0.34	0.87	0.37	0.91	0.33
a	0.78	0.76	0.81	0.73	0.54	0.45	1.04	0.44
y_0	0.02	0.06	0.05	0.09	0.11	0.11	0	0.2
p	<0.0001	<0.0001	<0.0001	0.0008	<0.0001	0.0004	<0.0001	0.0005
n	30	28	33	29	20	27	28	30

confidence intervals were small within the 2 to 10 mm depth range compared with those at the immediate vicinity of the sediment water interface and deep in the sediment. σ_X^2 and σ_Y^2 decreased from 0.031 and 0.025 close to the water-sediment interface to 0.005 and 0.004 mm^2 deep in the sediment, respectively (Figs. 10c, d). D_b^X and D_b^Y also decreased with depth (from 1.01 and 0.99 close to the sediment-water interface to 0.02 and 0.08 $cm^2.year^{-1}$ deep in the sediment, respectively) (Figs 11a, b). D_b^X and D_b^Y correlated significantly during all experiments (Table 3).

4. Discussion

a. Validation of the approach

To our knowledge, this is the first time that particle mixing fingerprints are experimentally assessed in a marine benthic invertebrate. Our results can therefore only be compared with: 1) qualitative knowledge regarding particle mixing induced by bivalves of the genus *Abra* (Grémare *et al.*, 2004; Maire *et al.*, 2006, 2007a, 2007b); and 2) assessments of τ_c and D_b^X derived from the application of CTRW models to vertical luminophore profiles recorded during experiments involving *Abra alba* (Braeckmann *et al.*, 2010).

The frequency distribution of the vertical component of particle jump lengths in *A. alba* is typically trimodal, with the first component oriented upward, the second oriented downward and the third one with a jump length close to zero. This result is in good agreement with the two kinds of luminophore movements identified by Maire *et al.* (2006) in both *A. ovata* and *A. nitida*. These authors showed that these two bivalves induce particle jumps through: 1) inhalant siphon displacements; and 2) shell motions due to the extension/retraction of the foot outside/inside the shell. During the present study, we observed an almost similar pattern in *A. alba*. The first kind of jumps are caused by the friction of the luminophores onto the siphon. Corresponding jumps can be either upward in case of siphon extension or downward in case of siphon retraction. Conversely, the jumps associated with foot extension/retraction have an almost zero length. During the present study, luminophore oscillations were also detected during maximal siphon extensions while foraging (inhalant siphon) or producing faeces (exhalant siphon), which creates temporary tensions on the sediment surrounding siphonal galleries. Also, slightly more complex, the pattern observed for *A. alba* is therefore coherent with the observed trimodal frequency distributions of the vertical component of jumps, which can be interpreted as resulting from the coexistence of: 1) shell induced oscillations and movements induced by siphon tension on the sediment; and 2) downward, and upward movements caused by siphons. This interpretation is further confirmed by the decrease of the mean absolute value of the vertical component of jump length with depth within the sediment column. This decrease indeed corresponds to an increase in the frequency of jumps with a null vertical length component at depth (i.e., in areas mostly affected by shell-associated jumps). Overall our results are thus consistent with the current qualitative knowledge regarding particle mixing in the genus *Abra*, which supports the validity of our assessments of jump characteristics.

Our assessment of particle mixing fingerprints can be compared with those derived from the fit of CTRW models to vertical luminophore profiles during experiments involving *A. alba* (Braeckman *et al.*, 2010). These authors reported D_b^X (i.e., 1D vertical D_b) between 0.96 and 4.47 $cm^2.y^{-1}$ vs. only 0.355 and 0.707 $cm^2.y^{-1}$ during our own experiments. Both ranges are low relative to literature data (Maire *et al.*, 2006, 2007a,b), which supports the apparently low intensity of particle mixing during our experiments (GB, personal observation). Our D_b^X values are slightly lower than those of Braeckman *et al.* (2010). Direct comparisons between the two studies are however complicated by several confounding factors. An important difference between the two experimental setups is the timing of the beginning of the experiment relative to luminophore introduction. Braeckman *et al.* (2010) started their experiments immediately after luminophore addition versus 24 hours later during the present study. Maire *et al.* (2007) emphasized that, due to the filling of large burrows or/and galleries, luminophores can be transferred to deep sediment layers immediately after their deposition at the sediment-water interface. They suggested that this could partly contribute to overestimates D_b^X during short-term experiments. Our own estimates of D_b^X are not affected by this bias, because: 1) they are based on experiments starting 24 hours after luminophore introduction; and 2) they are derived from the statistical analysis

of individual jumps. Consequently, the non-local (and non-directly associated with particle mixing) transfer of luminophores to deep sediment layers during their introduction at the sediment-water interface could explain some of the differences in the D_b^X recorded by Braeckman *et al.* (2010) and during the present study.

Braeckman *et al.* (2010) reported no significant effect of temperature, but a significant effect of density. They controlled this last factor by manipulating the number of clams within 10 cm internal diameter cores, whereas we monitored luminophore displacements over a much smaller spatial scale typically corresponding to the portion of sediment reworked by a single clam. It is therefore difficult to assess the exact clam density during our experiments, and discrepancies in the control of this factor may partly account for differences between the two studies.

While modelling vertical sediment profiles with CTRW models, Braeckman *et al.* (2010) used several assumptions regarding the frequency distributions of jump lengths (Gaussian distribution) and waiting times (Poisson process). Our own results suggest that these two distributions are not fully adequate to describe particle mixing in *A. alba*. Our results also show that the mean values of jump lengths and waiting times clearly decrease with depth within the sediment column. Meysman *et al.* (2008) showed that the types of *a priori* selected frequency distributions have a significant impact on the modelling of luminophore profiles, and thus possibly on D_b^X values. Here again, this could account for differences in D_b^X between our study and the one of Braeckman *et al.* (2010).

Another point is linked to the discrepancies between temporal scales classically associated with D_b^X measurements through modelling of luminophore profiles (i.e., 14 d for Braeckman *et al.* 2010) and with our approach (i.e., 10 s). Our results confirm the occurrence of oscillating jumps with an overall length close to zero as previously shown in other species of the genus *Abra* (Grémare *et al.*, 2004; Maire *et al.*, 2006). These jumps do not significantly affect luminophore profiles concentrations over temporal scales longer than their duration. They therefore do not significantly affect the assessment of D_b^X through the modelling of these profiles (De Baker *et al.*, 2011). Conversely, taking into account oscillating jumps do affect our own estimates of D_b^X, which could contribute to differences between our results and those of Braeckman *et al.* (2010).

Overall, the good compatibility of the frequency distributions of the vertical component of particle jumps recorded during the present study, with the current knowledge regarding the ethology of the genus *Abra* supports the validity of our approach. The comparison of our D_b^X with those derived by Braeckman *et al.* (2010) is less conclusive due to the existence of several confounding factors, which may account for differences between the two studies.

b. Limitations of the approach

Our approach is based on the use of two different algorithms, both relying on specific assumptions, which each induce limitations.

The first assumption, common to both algorithms, is linked with the use of thin aquaria coupled with image analysis techniques. It assumes that the information captured within the

monitored plane (two-dimensional) is representative of processes occurring in the three-dimensional sediment column. This assumption is most questionable for the assessment of jump characteristics. "Wall effects" may modify the trajectory of some jumps by constraining them to take place within the monitored plane. One can therefore not exclude a bias linked to the subsampling (i.e., within the monitored plane) of the jumps occurring in three-dimensional within the sediment column. We however believe this bias is weak for particle mixing induced by the genus *Abra* because, despite much higher D_b^X, Maire *et al.* (2006) have shown that luminophore profiles after 48 hours of experiment do not differ along the walls and within the whole sediment columns of thin aquaria containing *A. ovata*.

Another bias regarding waiting time measurements is the possibility of replacement of a luminophore by another luminophore, which would not be considered as a jump and can lead to an overestimation of waiting times. This probability can be approximated by the ratio of the surface occupied by luminophores to the total surface of sediment. During our experiments, this ratio was always less than 1%. Future experimentation should nevertheless consider the best threshold in luminophore concentrations: 1) to allow for the assessment of a high-enough number of jumps; and 2) not to bias the assessment of waiting times. One possibility consists in using multi-color tracers, which would allow to keep a similar overall luminophore concentration and to reduce the probability of replacement of a luminophore by another luminophore of the same color.

Image frequency acquisition and overall experiment duration are key parameters when assessing waiting times. It is not possible to detect waiting times shorter than the time interval between the acquisitions of two consecutive images (i.e., 10 s). This may result in an overestimation of mean waiting times. There are however good rationale to believe that this bias is negligible. In the genus *Abra*, particle mixing is mostly resulting from siphonal activity (Maire *et al.*, 2007b) and Grémare *et al.* (2004) have shown that a frequency acquisition of 0.05 Hz is sufficient to fully (i.e., $> 98\%$) describe this activity in *A. ovata*. Based on our own observations (OM and AG), particle mixing is clearly higher in *A. ovata* than in *A. alba*. We therefore believe that the image frequency acquisition used during the present study was appropriate to fully describe particle mixing in *A. alba*.

It is also not possible to measure a waiting time longer than overall experiment duration. The lack of recording of a waiting time can therefore be indicative of: 1) the total absence of jumps (*i.e.*, the total absence of particle mixing); and/or 2) the impossibility of sampling waiting times longer than experiment duration. Even for shorter waiting times, there is a bias towards the sampling of short waiting times using our approach. The probability that both the start and the end of a waiting period occur during a temporal window of a given duration indeed decreases with increasing waiting times. Although the number of long waiting times is clearly low in *A. alba*, this may lead to an underestimation of waiting times. During preliminary trials, we assessed the effect of experiment duration on the measurement of waiting times by comparing mean waiting times obtained by resampling the same experiment during overall durations comprised between one and 48 hours. Our results showed that mean waiting times: 1) tended to increase with experiment duration;

2) usually did not reach an asymptote within 48 hours; and 3) were affected by temporal changes in bivalve's activity. Our waiting time measurements were thus indeed affected by experiment duration. It should be stressed that such a dependency is also affecting other approaches currently used to assess particle mixing (Meysman *et al.*, 2010). Anyhow, experiment duration should carefully be adjusted when using our approach and special care must be taken to carry out long-term experiments when: 1) particle mixing is low; and/or 2) not constant relative to time.

The assessment of jump characteristics requires that a luminophore remains visible within the monitored plane during the entirety of its jump. This is clearly not the case in a large variety of sediment remixing modes, including non-local movements associated with feeding and/or particle transfers within animals' guts or even biogenic structures such as burrows and tubes. The approach described in the present study is not adequate for those types of particle mixing, which include both downward and upward conveyors (François *et al.*, 1997, 2002).

Even when the luminophore remains visible during the entirety of its jump, our approach requires that its consecutive positions remain close enough for the reconstruction of its trajectory. The algorithm used for the assessment of jump characteristics is indeed using two circles (*i.e.*, the sensitivity and the search circles) centered on the initial position of the luminophore. The reconstruction of luminophore movements requires that the second of two consecutive positions of the luminophore is located outside the sensitivity and inside the search circle. For quick non-local displacements, this can be achieved by increasing the size of the search circle and/or image frequency acquisition. Increase in the size of the search circle is limited because it would result in too many luminophores to be included (i.e., too many possible ending points of elementary displacements), which would complicate trajectory assessment. Increasing image frequency acquisition would result in much larger image files, not compatible with our current possibilities of image processing. In this last case, it is however possible to subsample these files and to derive the distributions regarding the characteristics of jump length from the analysis of these subsamples. There is indeed no *a priori* reason to suspect that the so-determined distributions would not be representative of those which could have been derived from the analysis of the whole file.

Overall, the approach presented during the present study is suitable to assess particle mixing in animals moving sediment particles frequently and over relatively short distances (or over larger distances but slowly). It therefore appears mainly appropriate for the biodiffusors and the gallery-diffusors groups, and is possibly transposable to regenerators (François *et al.*, 1997, 2002). Because of such restrictions in its applicability, this approach does not seem appropriate to assess particle mixing by benthic communities as a whole. The direct extrapolation of our results to field populations may itself prove difficult due to density (Braeckman *et al.* 2010), individual size (Wikander 1980) and temperature (Maire *et al.* 2007c) in the genus *Abra*. Conversely, our approach is highly suitable to assess the effects of these factors and of their interactions during laboratory experiments, which would allow for the indirect assessment of sediment mixing by field populations.

c. Particle mixing fingerprints in Abra alba

i. *Vertical and horizontal components of particle mixing.* The positive correlations between D_b^X and D_b^Y suggest that the vertical and horizontal components of particle mixing are both cued by the same process, namely: clam activity as already shown by Maire *et al.* (2007b) for *A. ovata*. Corresponding slopes were between 0.45 and 1.05 with a mean of 0.69, which suggests that the horizontal and the vertical components of particle mixing induced by *A. alba* are of the same order of magnitude. This observation is consistent with the rough estimates derived by Wheatcroft *et al.* (1990), which led these authors to state that the horizontal components of particle mixing induced by benthic invertebrates exceed vertical ones. Based on the relationships between D_b^X and D_b^Y; and the direction of particle displacements proposed by Wheatcroft *et al.* (1990), this also suggests that, in *A. alba* the mean angle of particle jump direction with the vertical should be close to 40° (45° during Exp. 3). Interestingly, during this last experiment, we recorded a preferential range of jump direction between 180 and 270°, centered around 225°, which corresponds to downward jumps oriented 45° from the vertical. This pattern mostly resulted from the orientation of the siphonal galleries preferentially used during the experiment. Over short time scales, changes in the ratio between horizontal and vertical components of sediment reworking thus appears to be mainly controlled by the orientation of preferential siphonal galleries. Our own observations show that the position of the siphon of *A. alba* changes while exploring different sectors of the sediment. Therefore, over longer time scales, changes in this ratio would probably be mainly controlled by the general geometry of the siphonal galleries network. In this last case, one would expect this ratio to become less variable between individuals/experiments, which could be tested by carrying out longer-term experiments.

ii. *Spatial heterogeneity of particle mixing fingerprints*. Particle mixing induced by *A. alba* was spatially heterogeneous. The analysis of the spatial distribution of waiting times during Experiment 3 allows for the distinction between four areas:

1) The sediment-water interface, where particle mixing is high and mostly consists in sediment movements induced by the distal part and the tip of the inhalant siphon. This area is characterized by the shortest values of waiting times and the highest values of both the horizontal and vertical components of jump vectors. It is also characterized by the highest normalized number of jumps. Its overall thickness is ca. 2.5mm.
2) The network of siphonal galleries, which has a conical shape and an overall volume of ca. 2,700 mm^3 resulting in a surface of ca. 200 mm^2 in the monitored plane. This area is characterized by intermediate and highly variable waiting times and jump lengths resulting from the preferential use of two siphonal galleries during the period under study. Overall, particle mixing is highly heterogeneous within this area.

3) Two subsurface areas located outside the network of siphonal galleries, which are characterized by very long waiting times. These two areas are ca. 12mm^2 and are located on both sides of the monitored field. Based on experimental data by Maire *et al.* (2007a), Meysman *et al.* (2008a) stated that the vertical luminophore profiles generated by *A. ovata* consisted in two separate zones: an upper "blocky zone" where particles movements are few due to restricted access by the inhalant siphon, and a lower "smooth zone" where particles movements due to siphon activity take place. According to Meysman *et al.* (2008b) these "blocky zones" are due to lateral heterogeneity in particle mixing. During the present study, we have worked at a small spatial scale (i.e., a few cm) typically associated with a single bivalve. Our results nevertheless show the occurrence of subsurface areas characterized by low particle mixing activity, which could be considered as the extension of interface "blocky zones" (Meysman *et al.*, 2008a).
4) The area immediately surrounding the shell, which is characterized by low horizontal components of jump vectors and low variability in both the horizontal and vertical components of jump vectors. This corresponds to the strong dominance of almost vertical jumps resulting from the protrusion/retraction of the foot inside/outside the shell.

The relative importance of these four areas and associated particle mixing processes varies with depth within the sediment column, which induces vertical changes in particle mixing fingerprints. The vertical profile of mean waiting times is characterized by a subsurface maximum in relation with: 1) high particle mixing activity at the sediment-water interface due to intense foraging by the inhalant siphon (see point 1 above); and 2) the occurrence of the two subsurface areas located outside the siphonal gallery network and characterized by almost null particle mixing activity (see point 3 above). Conversely, the vertical profiles of mean absolute values of jump vectors and of σ_X^2 and σ_Y^2 are all characterized by maximal values at the sediment-water interface and then a continuous decline with depth. This corresponds to the occurrence of: 1) long jumps associated with siphon movements close to the sediment-water interface,; and 2) a decrease in the variety of jumps with depth in the sediment column. The vertical profiles of D_b^X and D_b^Y are also characterized by maximal values (ca. 10 times higher than 2 cm deep in the sediment) at the sediment-water interface and then by a continuous decrease wit depth within the sediment column. They are therefore more similar to the vertical profiles of σ_X^2 and σ_Y^2 than to the vertical profile of waiting times. This suggests that vertical changes in D_b^X and D_b^Y are more cued by changes in jump characteristics than waiting time.

d. Consequences for the use of CTRW models in Abra alba

i. *Suitability of the distributions classically used in CTRW to describe particle mixing in A. alba.* CTRW models are currently used to assess D_b^X (through mean waiting

times and σ^2) based on their fits to vertical luminophore profiles. This approach requires that the frequency distributions can be described by simple functions and characterized by a limited number of parameters. The most often used functions for describing the frequency distributions of waiting times and jump lengths are the Poisson process and the Gaussian distribution (Maire *et al.*, 2007a; Braeckman *et al.*, 2010; De Backer *et al.*, 2011). The question of the choice of these functions was recently discussed by Meysman *et al.* (2008b). This selection is made *a priori* without quantitative information regarding their pertinence to particle mixing behaviour. To our knowledge, the present study is the first one, which allows for the direct assessment of those distributions.

Our results support the "long right tail shape" of waiting times distributions, proposed by Meysman *et al.* (2008a, 2008b, 2010). However, they also show that the fit of the Poisson process to the frequency distributions of waiting times is quite approximate (Table 1). In spite of the undersampling of long waiting times, the frequency distributions of waiting times were indeed less dominated by very short waiting times than those derived using the Poisson process. Moreover, τ_c derived from fitting according to a Poisson process were always smaller than directly calculated T_c. Our results therefore suggest the Poisson process is not fully suitable to describe the frequency distribution of waiting times in *A. alba*.

The vertical jump length frequency distributions recorded during the present study exhibited three modes, each associated with specific shell or siphon movements. This is rather different from the Gaussian distribution generally assumed in CTRW (Meysman *et al.* 2008a, 2008b, 2010) and proposed by Meysman *et al.* (2008b) for a "burrowing" bivalve. These authors also proposed a more complex (*i.e.*, with two modes) frequency distribution for a "deposit feeding worm." By simple combination of these two distributions, one could thus expect that a benthic community composed of these two types of organisms would induce a trimodal frequency distribution of vertical components of jump vectors. Our results show that such a complex distribution can also result from different particle movements induced by a single species. In any case, the Gaussian distribution is not fully suitable to describe the frequency distribution of the vertical component of jump vectors in *A. alba*.

Overall, it appears that the particle mixing fingerprints experimentally measured during the present study do not follow the CTRW model most often used distributions. Further applications of the CTRW model should therefore include preliminary checks of the adequacy of these distributions to the species/communities studied.

ii. *Taking into account spatial heterogeneity when modelling particle mixing in A. alba.* The 1D-CTRW mixing model assumes that the frequency distributions of waiting times and jump characteristics do not vary spatially (Meysman *et al.*, 2008a). Our results show that this is not the case in *A. alba*. Lateral heterogeneity in particle mixing fingerprints mainly results from the occurrence of areas characterized by restricted access to the inhalant and exhalant siphons. According to our observations,

the preferential localisations of the siphons are changing with time. Our results thus support the hypothesis of Meysman *et al.* (2008b), who stated that, due to bivalve's relocation, lateral heterogeneity in particle mixing should become negligible with increasing experiment duration. One way of handling lateral variability would thus be to use experimentally determined particle mixing fingerprints provided that they are derived from long-enough experiments to result in horizontally homogeneous particle mixing.

As far as vertical heterogeneity is concerned, our results show: 1) a clear increase of waiting times with depth within the sediment column; 2) more frequent vertical jumps deep in the sediment column; and 3) shorter jump lengths deep in the sediment column. These patterns resulted in lower D_b^X as depth within the sediment column increases. This is linked to the morphology and the ethology of *A. alba* and there is therefore no reason to believe that vertical heterogeneity would diminish with experiment duration. Taking into account vertical heterogeneity in CTRW models would therefore require to introduce a discretisation relative to depth and to use different particle mixing fingerprints for each of the so-defined depth intervals.

iii. *Consequences on the use of CTRW models.* An important point consists in assessing to what extent the weaknesses of the frequency distributions classically used in CTRW models indeed affect the assessment of particle mixing fingerprints. In *A. alba*, this could be achieved by: 1) running a "classical" CTRW model on our experimental data and comparing its outputs with our own overall mean D_b^X; and 2) comparing the relative ability of a "classical" and an "experimentally based" CTRW model to describe our experimental data. Depending on the outcome, one could conclude on the validity of future use of classical CTRW models to assess particle mixing in *A. alba*. In case of similar outputs, this conclusion will not necessarily hold for other organisms, especially those belonging to other particle mixing groups. In case of different outputs, one will have to unravel the effects linked to the selection of distributions and spatial heterogeneity. In any case, this will make the use of CTRW to infer particle mixing hazardous due to: 1) the necessary *a priori* knowledge regarding the shape of (simple enough) distributions; and/or 2) the level of complexity associated with the description of spatial (mostly vertical) heterogeneity.

e. Temporal dynamics and possible coupling with other innovative approaches

Although not fully developed during the present study, our approach allows for the assessment of particle mixing dynamics in two-dimensions, which opens the field for a coupling with other emerging techniques for the study of biogeochemical processes taking place at the sediment-water interface. This could, for example, include the coupling with other non-invasive two-dimensional imaging systems such as planar optodes (Volkenborn *et al.* 2012) or Diffusion Gradient Thin gels (Teal *et al.* 2012) to better assess how the interactions between ethology, particle mixing, bioirigation, oxygen and metals spatio-temporal distributions are controlled by environmental factors such as temperature and POM availability.

Acknowledgments. This work is part of the Ph.D. thesis of G. Bernard (University Bordeaux 1). He was supported by a doctoral grant from the French "Ministère de l'Enseignement Supérieur et de la Recherche.' This work was funded through the BIOMIN (LEFE-CYBER and EC2CO-PNEC), the "Diagnostic de la Qualité des Milieux Littoraux" and the " OSQUAR " (Conseil Régional Aquitaine) programs. It was supported by a VIDI grant from the Netherlands Organization for Scientific Research (NWO) to FJRM and contributes to the Darwin Institute for Biogeosciences.

REFERENCES

Aller, R. C. 1982. The effects of macrobenthos on chemical properties of marine sediment and overlying water, in Animal-Sediment Relations, P. L. McCall and P. J. S. Tevesz, ed., Plenum, New York, 53–102.

Aller, R. C. and J. Y. Aller. 1998. The effect of biogenic irrigation intensity and solute exchange on diagenetic reaction rates in marine sediments. J. Mar. Res., *52*, 905–936.

Backer De; A., F. Coillie Van; F. Montserrat; P. Provoost; C. Colen Van; M. Vincx and S. Degraer. 2011. Bioturbation effects of *Corophium volutator*: Importance of density and behavioural activity. Est. Coast. Shelf. Sci., *91*, 306–313.

Blanchet, H.; X. de Montaudouin; P. Chardy and G. Bachelet. 2005. Structuring factors and recent changes in subtidal macrozoobenthic communities of a coastal lagoon, Arcachon Bay (France). Est. Coast. Shelf. Sci., *64*, 561–576.

Borja, A.; F. Aguirrezabalaga; J. Martínez; J. C. Sola; L. García-Arberas and J. M. Gorostiaga. 2004. Benthic communities, biogeography and resources management, in Oceanography and marine environment of the Basque Country, A. Borja, M.Collins M, ed., Elsevier Oceanogr. Ser., *70*, 455–492.

Boudreau, B. P. 1986a. Mathematics of tracer mixing in sediments: I. Spatially-dependent, diffusive mixing. Am. J. Sci., *286*, 161–198.

Boudreau, B. P. 1986b. Mathematics of tracer mixing in sediment: II. Non-local mixing and biological conveyor-belt phenomena. Am. J. Sci., *286*, 199–238.

Boudreau, B. P. 1997. A one-dimensional model for bed-boundary layer particle exchange. J. Mar. Syst., *11*, 279–303.

Boudreau, B. P. and D. M. Imboden. 1987. Mathematics of tracer mixing in sediments. III. The theory of nonlocal mixing within sediments. Am. J. Sci., *287*, 693–719.

Braeckman, U.; P. Provoost; B. Gribsholt; D. Van Gansbeke; J. J. Middelburg; K. Soetaert; M. Vincx and J. Vanaverbeke. 2010. Role of macrofauna functional traits and density in biogeochemical fluxes and bioturbation. Mar. Ecol. Prog. Ser., *399*, 173–186.

Choi, J.; F. François-Carcaillet and B. P. Boudreau. 2002. Lattice-automaton bioturbation simulator (LABS): implementation for small deposit feeders. Comput. Geosci., *28*, 213–222.

Delmotte, S.; F. J. R. Meysman; A. Ciutat; A. Boudou; S. Sauvage and M. Gérino. 2007. Cadmium Transport in Sediments by Tubificid Bioturbation: an Assessment of Model Complexity. Geochim. Cosmochim. Acta., *71*, 844–862.

François, F.; J. C. Poggiale; J. P. Durbec and G. Stora. 1997. A new approach for the modelling of sediment reworking induced by a macrobenthic community. Acta. Biotheor., *45*, 295–319.

François, F.; M. Gérino; G. Stora; J. P. Durbec and J. C. Poggiale. 2002. Functional approach to sediment reworking by gallery-forming macrobenthic organisms: modeling and application with the polychaete *Nereis diversicolor*. Mar. Ecol. Prog. Ser., *229*, 127–136.

Gérino, M.; R. C. Aller; C. Lee; J. K. Cochran; J. Y. Aller; M. A. Green and D. Hirschberg. 1998. Comparison of different tracers and methods used to quantify bioturbation during a spring bloom: 234-Thorium, luminophores and chlorophyll a. Estuar. Coast. Shelf. Sci., *46*, 531–547.

Gilbert, F.; P. Bonin and G. Stora. 1995. Effect of bioturbation on denitrification in a marine sediment from the West Mediterranean littoral. Hydrobiologia, *304*, 49–58.

Gilbert, F.; S. Hulth, N. Stroemberg; K. Ringdahl and J. C. Poggiale. 2003. 2-D optical quantification of particle reworking activities in marine surface sediments. J. Exp. Mar. Biol. Ecol., *285/286*, 251–263.

Grémare, A.; J. C. Duchêne; R. Rosenberg; E. David and M. Desmalades. 2004. Feeding behaviour and functional response of *Abra ovata* and *A. nitida* compared by image analysis. Mar. Ecol. Prog. Ser., *267*, 195–208.

Guinasso, N. L. and D. R. Schink. 1975. Quantitative estimates of biological mixing in abyssal sediments. J. Geophys. Res., *80*, 3032–3043.

Hughes, T. G. 1975. The sorting of food particles by *Abra* sp. (Bivalvia: Tellinacea). J. Exp. Mar. Biol. Ecol., *20*, 137–15.

Kristensen, E. 2000. Organic matter diagenesis at the oxic/anoxic interface in coastal marine sediments, with emphasis on the role of burrowing animals. Hydrobiologia, *426*, 1–24.

Kristensen, E.; G. Penha-Lopes; M. Delefosse; T. Valdemarsen; C. O. Quintana and G. Banta. 2012. What is bioturbation? The need for a precise definition for fauna in aquatic sciences. Mar. Ecol. Prog. Ser., *446*, 285–302.

Lecroart, P.; S. Schmidt and J. M. Jouanneau. 2007. Numerical estimation of the error of the biodiffusion coefficient in coastal sediments. Est. Coast. Shelf. Sci., *72*, 543–552.

Lecroart, P.; O. Maire; S. Schmidt; A. Grémare; P. Anschutz and F. J. R. Meysman. 2010. Bioturbation and short lived radioisotopes. Geochim. et Cosmochim. Acta., *74*, 6049–6063.

Lohrer, A. M.; S. F. Thrush; M. M. Gibbs. 2004. Bioturbators enhance ecosystem function through complex biogeochemical interactions. Nature, *431*, 1092–1095.

Maire, O.; J. C. Duchêne; R. Rosenberg; J. Braga de Mendonça Jr. and A. Grémare. 2006. Effects of food availability on sediment reworking in *Abra ovata* and *Abra nitida*. Mar. Ecol. Prog. Ser., *319*, 135–153.

Maire, O.; J. C. Duchêne; A. Grémare; V. S. Malyuga and F. J. R. Meysman. 2007a. A Comparison of sediment reworking rates by the Surface Deposit-Feeding Bivalve *Abra Ovata* during summertime and wintertime, with a comparison between two models of sediment reworking. J. Exp. Mar. Biol. Ecol., *343*, 21–36.

Maire, O.; J. C. Duchêne; L. Bigot and A. Grémare. 2007b. Linking feeding activity and sediment reworking in the deposit-feeding bivalve *Abra ovata* with image analysis, laser telemetry, and luminophores tracers. Mar. Ecol. Prog. Ser., *351*, 139–150.

Maire, O.; J. C. Duchêne; J. M. Amouroux and A. Grémare. 2007c. Activity patterns in the terebellid polychaete *Eupolymnia nebulosa* assessed using a new image analysis system. Mar. Biol., *151*, 737–749.

Maire, O.; P. Lecroart; F. J. R. Meysman; R. Rosenberg; J. C. Duchêne and A. Grémare, 2008. Methods of sediment reworking assessment in bioturbation research: a review. Aquat. Biol., *2*, 219–238.

Meadows, P. S. and A. Meadows. 1991. The geotechnical and geochemical implications of bioturbation in marine sedimentary ecosystems. Symp. Zool. Soc. Lond., *63*, 157–181.

Meysman, F. J. R.; B. P. Boudreau and J. J. Middelburg. 2003. Relations between local, nonlocal, discrete and continuous models of bioturbation. J. Mar. Res. *61*, 391–410.

Meysman, F. J. R.; J. J. Middelburg and C. H. R. Heip. 2006. Bioturbation: a fresh look at Darwin's last idea. Trends. Ecol. Evol. *12–21*, 688–695.

Meysman, F. J. R.; V. S. Malyuga; B. P. Boudreau and J. J. Middelburg. 2008a. A generalized stochastic approach to particle dispersal in soils and sediments. Geochim. Cosmochim. Acta, *72*, 3460–3478.

Meysman, F. J. R.; V. S. Malyuga; B. P. Boudreau and J. J. Middelburg. 2008b. Quantifying particle dispersal in aquatic sediments at short time scales: model selection. Aquat. Biol. *2*, 239–254.

Meysman, F. J. R.; B. P. Boudreau and J. J. Middelburg. 2010. When and why does bioturbation lead to diffusive mixing? J. Mar. Res. *68*, 881–920.

Pearson, T. and R. Rosenberg. 1978. Macrobenthic succession in relation to organic enrichment and pollution of the marine environment. Oceanogr. Mar. Biol. Annu. Rev., *16*, 229–331.

Piot, A.; A. Rochon; G. Stora and G. Desrosiers. 2008. Experimental study on the influence of bioturbation performed by *Nephtys caeca* (Fabricius) and *Nereis virens* (Sars) annelidae on the distribution of dinoflagellate cysts in the sediment. J. Exp. Mar. Biol. Ecol., *359*, 92–101.

Reed, D. C.; K. Huang; B. P. Boudreau and F. J. R. Meysman. 2006. Steady-state tracer dynamics in a lattice-automaton model of bioturbation. Geochim. Cosmochim. Acta, *70*, 5855–5867.

Rhoads, D. C. 1974. Organism-sediment relations on the muddy seafloor. Oceanogr. Mar. Biol. Ann. Rev., *12*, 263–300.

Rhoads, D. C. and L. F. Boyer. 1982. The effects of marine benthos on physical properties of sediments. A successional perspective, in Animal–sediment relations—the biogenic alteration of sediments. Topics in geobiology, Vol 2, P. L. McCall, M. J. S. Tevesz, ed., Plenum, New York, 3–52.

Rice, D. L. 1986. Early diagenesis in bioadvective sediments: relationships between the diagenesis of beryllium-7, sediment reworking rates, and the abundance of conveyorbelt deposit-feeders. J. Mar. Res., *44*, 149–184.

Robbins, J. A. 1986. A model for particle-selective transport of tracers in sediments with conveyor-belt deposit feeders. J. Geophys. Res. *91*, 8542–8558.

Rosenberg, R. 1993. Suspension feeding in *Abra alba* (Mollusca). Sarsia, *78*, 119–121

Rowden, A. A.; C. F. Jago and S. E. Jones. 1998. Influence of benthic macrofauna on the geotechnical and geophysical properties of surficial sediment, North Sea. Cont. Shelf. Res., *18*, 1347–1363.

Shull, D. H. 2001. Transition-Matrix Model of Bioturbation and Radionuclide Diagenesis. Limnol. Oceanogr., *46*, 905–916.

Shull, D. H. and M. Yasuda. 2001. Size-selective downward particle transport by cirratulid polychaetes. J. Mar. Res., *59*, 453–473.

Soetaert, K; P. M. J. Herman; J. J. Middelburg; C. Heip; H. S. De Stigter; T. C. E. Van Weering; E. Epping and W. Helder. 1996. Modelling ^{210}Pb-derived mixing activity in ocean margin sediments: diffusive versus non local mixing. J. Mar. Res., *54*, 1207–1227.

Solan, M.; B. D. Wigham; I. R. Hudson; R. Kennedy; C. H. Coulon; K. Norling; H. C. Nilsson and R. Rosenberg. 2004. In Situ Quantification of Bioturbation Using Time-Lapse Fluorescent Sediment Profile Imaging (F-Spi.), Luminophore Tracers and Model Simulation. Mar. Ecol. Prog. Ser. *271*, 1–12.

Teal, L. R.; E. R. Parker and M. Solan. 2012. Simultaneous quantification of in-situ infaunal activity and pore-water metal concentrations: establishment of benthic ecosystem process-function relations. Biogeosciences Discuss., *9*, 8541–8570.

Van Hoey, G.; M. Vincx and S. Degraer. 2005. Small-scale geographical patterns within the macrobenthic *Abra alba* community. Est. Coast. Shelf. Sci., *64*, 751–763.

Volkenborn, N.; L. Polerecky; D. S. Wethey; T. H. DeWitt and S. A. Woodin. 2012. Hydraulic activities by gost shrimp *Neotrypaea californiensis* induce oxic-anoxic oscillations in sediment. Mar. Ecol. Prog. Ser., *455*, 141–156.

Wheatcroft, R. A.; P. A. Jumars; C. R. Smith and A. R. M. Nowel. 1990. A mechanistic view of the particulate biodiffusion coefficient: rest periods and transport directions. J. Mar. Res., *48*, 177–201.

Wheatcroft, R. A. 1992. Experimental tests for particle size-dependent bioturbation in the deep ocean. Limnol. Oceanogr., *37*, 90–104.

Wikander, P. B. 1980. Biometry and behaviour in Abra nitida (Müller) and A. longicallus (Scacchi) (Bivalvia, Tellinacea). Sarsia, *65*, 255–268.

Received: *May 30, 2012*; revised: *Dec. 14, 2012*.